Chemical Engineering Journal 159 (2010) 236–241

Contents lists available at ScienceDirect

Chemical Engineering Journal

journal homepage: www.elsevier.com/locate/cej

Chlorination of titanium carbide for the processing of nanoporous carbon: A kinetic study

Philipp Becker, Friedrich Glenk, Martina Kormann, Nadejda Popovska, Bastian J.M. Etzold*

Universität Erlangen-Nürnberg, Lehrstuhl für Chemische Reaktionstechnik, Egerlandstr. 3, 91058 Erlangen, Germany

ARTICLE INFO

Article history:
Received 15 December 2009
Received in revised form 4 February 2010
Accepted 5 February 2010

Keywords:
Kinetics
Carbide-derived carbon
Titanium carbide
Nanoporous carbon

ABSTRACT

Nanoporous carbon synthesized via the chlorination of titanium carbide at temperatures above 400 °C shows a good performance, e.g. for gas storage or electrochemical applications. In this work the influence of the temperature and of the chlorine concentration on the reaction rate and the development of the porous structure during the course of the reaction was studied. The synthesis follows a Langmuir–Hinshelwood approach regarding chlorine, which can be simplified to a power law rate with the order of 0.71, and the specific surface area is created mainly in the last 10% of conversion.

1. Introduction

Microporous carbons are widely employed in the field of chemical engineering. Fields of applications are for example waste water treatment, gas purification or catalysis [1–5]. Although being known for decades, the interest of science and industry in porous carbons is unbroken. For the present challenges in the energy sector these materials are in discussion for several applications, like for example the employment as adsorbent to improve the storage of hydrogen and natural gas or electrochemical applications like materials for double layer capacitors or catalyst support material for fuel cells. Recent success in producing carbons with specific surface areas above 3000 m^2/g increased the effectiveness of these materials.

Some methods for the synthesis of porous carbons are well-known and already industrially employed, e.g. the activation of carbon with phosphoric acid or carbon dioxide [1], but also new methods are in the focus of actual research. One of them is the synthesis of microporous carbon with narrow and adjustable pore size distribution by the chlorination of metallic carbides and is known as carbide-derived carbon (CDC) method [6]. The reaction is performed at elevated temperatures, where the non-carbon compound of the carbide reacts with chlorine to a gaseous species, while the carbon remains as a solid phase. For the chlorination of titanium carbide the overall reaction equation is:

$$TiC(s) + 2Cl_2(g) \rightarrow TiCl_4(g) + C(s)$$

Temperatures above 400 °C are necessary to suppress the formation of CCl_4, which would result in a loss of carbon. Gogotsi et al. showed that the synthesis of CDC materials has two technical advantages [7,8]. The overall shape of the carbide is retained during the chlorination, and thus the shape of the resulting carbon can be influenced by the precursor carbide and no shrinkage, like common for pyrolysis, occurs. Secondly, the resulting pore size distribution can be adjusted by the precursor carbide and the chlorination temperature [8–10].

Carbide-derived carbon synthesized by the chlorination of titanium carbide (abbreviated in this work TiC-DC) show extraordinary performance in the application as adsorbent material [11–16] and the field of electrochemistry [17–24]. Beside these fields also the employment as tribological coatings, antimicrobial material or membranes are discussed in literature [6,25–27]. Despite good performance and detailed studies on the resulting pore structure, up to now, to our best knowledge, no detailed studies of the kinetics of the synthesis of TiC-DC are reported in the literature. Some kinetics are presented for the related process of the chlorination of silicon carbide by various authors [28–32]. But for TiC-DC detailed kinetic data are still unknown, although they are essential for the design of industrial synthesis processes.

This work presents a kinetic study on the chlorination of commercial titanium carbide powders.

2. Experimental

Commercial titanium carbide powder (99.5% purity, approximately 3.5 μm in diameter, Alfa Aesar GmbH & Co. KG) was chosen as carbide precursor. The chlorination was performed in a

* Corresponding author. Tel.: +49 9131 8527430; fax: +49 9131 8527421.
E-mail address: bastian.etzold@crt.cbi.uni-erlangen.de (B.J.M. Etzold).

1385-8947/$ – see front matter © 2010 Elsevier B.V. All rights reserved.
doi:10.1016/j.cej.2010.02.011

Table 1
Reaction conditions for the chlorination of TiC.

Temperature	400–1200 °C
Total pressure	98 kPa
Chlorine concentration	0.22–6.7 mol/m^3
Superficial velocity	0.015–0.045 m/s
Etching time	10–120 min

horizontal tubular reactor heated by a furnace (Gero Company). The alumina tube was 1300 mm in length and 32 mm in diameter. Temperature profiles were taken to determine the isothermal zone and adjust the controller of the furnace. All gases were dosed via mass flow controllers. The exhaust gas was cleaned by a cooling trap and by absorption in a 30% potassium hydroxide solution.

To perform the chlorination approximately 0.5 g of the titanium carbide powder was filled into a ceramic crucible, which was placed in the isothermal zone of the reactor. To check tightness and to remove oxygen, the reactor was evacuated and then filled with helium. Thereafter, the reactor was heated up to 600 °C and the samples were exposed to a He/H_2 atmosphere (16.7 vol.% H_2) for 30 min. The chlorination temperature and superficial velocity were set during a further purge with helium. After the selected final temperature was reached the reaction was started by switching to a chlorine/helium mixture. The reaction was stopped by flushing with pure helium. Traces of chlorine adsorbed on the porous carbon the substrate were removed by flushing with a H_2/He mixture for 30 min at 600 °C.

The reaction progress was determined gravimetrically, i.e. the mass of the precursor carbide was measured before the experiment and after the reaction (after the reactor had been cooled down). Partially reacted carbides were not further used for the kinetic study, i.e. the reaction time was varied based on experiments with fresh TiC. If it is assumed that the recorded loss of mass results only from titanium, which is etched from the carbide, hence that no carbon is etched and that no re-deposition occurs, the total etching rate r_{total} and the degree of conversion X can be calculated by:

$$r_{total} = \frac{\Delta m}{M_{Ti} \cdot t \cdot m_0} (\text{mol/kg s}) \quad (1)$$

$$X(t) = \frac{n_{0,TiC} - n_{TiC}(t)}{n_{0,TiC}} = \frac{n_{0,Ti} - n_{Ti}(t)}{m_{0,TiC}/M_{TiC}} = \frac{m_{0,TiC} - m_{CDC,TiC(t)}/M_{Ti}}{m_{0,TiC}/M_{TiC}} \quad (2)$$

with t: the time in s; n_0, m_0: initial amount of substance or mass in mol or kg; $n_{Ti}(t)$: amount of substance in mol of Ti remaining in the CDC/carbide substrate after reaction time t; $m_{CDC,TiC}(t)$: mass of remaining CDC/carbide substrate after reaction time t in kg; M: molar mass in kg/mol.

To determine the kinetic parameters (reaction order, activation energy, pre-exponential factor) the reaction time, the temperature and the initial chlorine concentration were varied (Table 1). Beside the gravimetric monitoring of the reaction progress, the materials were also analyzed by means of N_2- and CO_2-sorption measurements (Quantachrome QuadrasorbSi-MP and Nova 4200e) and by the determination of the true density (Porotec Pycnomatic Multivolume). For the evaluation of the sorption measurements the NL-DFT model for carbons with slit pores (software QuadraWin 4.01 and NovaWin 10.0) was employed. Raman spectra were recorded from 100 to 3000 cm^{-1} (Raman spectrometer Dilor ISA Labram HR) equipped with a HeNe laser (k = 633 nm) at 50× magnification.

3. Results and discussion

3.1. Influence of reaction time

Degrees of conversion of the titanium carbide between approximately 10 and 90% were achieved by variation of the reaction time

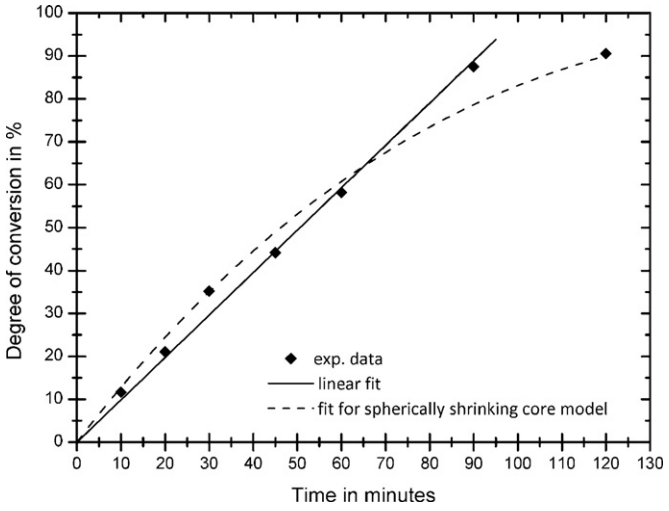

Fig. 1. Degree of conversion of TiC versus reaction time ($c_{Cl_2,0}$ = 0.45 mol/m^3, 800 °C).

in a range of 10–120 min at 800 °C and 0.45 mol/m^3 of chlorine. XRD-analysis of the raw material shows crystalline titanium carbide. From particle size measurements it is known that the mean particle size is 3.5 μm and that 92 vol.% of the particles are smaller than 9.3 μm, while the maximum measure particle size was 24 μm. From N_2-sorption measurement the specific surface area (BET) of the raw material results to 1.1 m^2/g. Comparison of the particle size distribution of the original and the chlorinated powder showed no change in the particle size. Hence the shape of the carbide particles is retained during the chlorination. Fig. 1 shows the plot of conversion versus reaction time. The conversion of TiC increases almost linearly up to 87% conversion is reached after 90 min. Thereafter the conversion increases only very slowly, and the reaction rate drops strongly. The conversion of chlorine is relatively small (<40%) and additionally due to the volume consuming reaction the concentration of chlorine does not decrease more than 25% (see Chapter 3.3). Thus for the subsequent discussion it is assumed that the chlorine concentration within the reactor and the crucible, respectively, can be represented by the mean value of the inlet and outlet concentration. During the conversion of the titanium carbide powder a porous carbon layer between the gas phase and the reactive carbide/carbon interface develops and is growing continuously. Thus the reactive interface area may change during the course of the reaction.

The linear development of the degree of conversion over the time in the first region (X_{TiC} < 90%) indicates that the growing porous carbon layer does not induce pore diffusion limitations, because the reaction rate would then decrease strongly with increasing layer thickness and TiC conversion, respectively. Thus the rate should be proportional to the reactive interfacial area between carbon and carbide; which may change during the course of reaction. The border case where this influence is pronounced most, is a spherical substrate, where the change of the reactive surface with time is given by:

$$A(t) = z \cdot \pi \cdot (d(t))^2 \quad (3)$$

$$d(t) = \sqrt[3]{\frac{1}{\pi \cdot z} \cdot V_0 \cdot (1 - X(t)) \cdot 6} = \sqrt[3]{d_0^3 \cdot (1 - X)} \quad (4)$$

$$\Rightarrow A(t) = z \cdot \pi \cdot (d_0^3 \cdot (1 - X))^{2/3} \quad (5)$$

with z: number of spherical particles; d_0: initial diameter of the spherical particles in m; A: reactive interface area; V_0: initial volume of a single spherical particle in m^3.

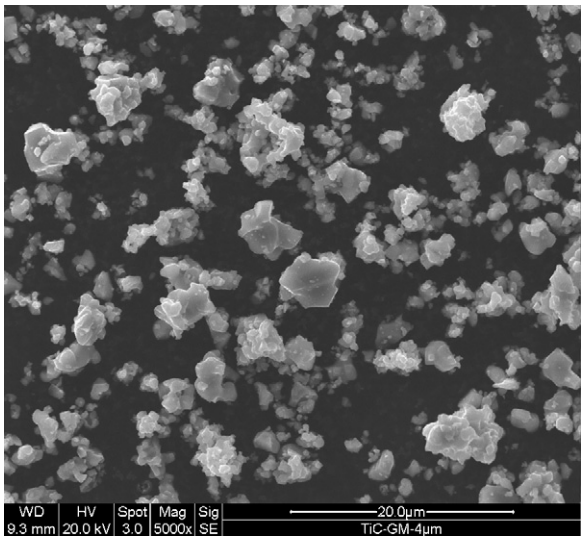

Fig. 2. SEM image of the untreated titanium carbide powder.

With the assumption of a mean (constant) chlorine concentration, the rate of the TiC conversion is given by:

$$\frac{dX}{dt} = A(t) \cdot k_X \cdot \overline{c_{Cl_2}} = A(t) \cdot k'_X|_{X \leq 1} \tag{6}$$

with k_X: reaction rate constant in %m/s/mol; k'_X: pseudo reaction rate constant in %/s/m^2.

Eqs. (5) and (6) can be solved by the integration of Eq. (6) in small time increments that account for the degree of TiC conversion and changing surface area at each integration step. The number z of the spherical particles was calculated from the initial mass, the carbide density and the mean substrate diameter. The pseudo reaction rate constant k' was used as the fitting parameter. Fig. 1 shows the respective fit following the shrinking core model for spherical particles and also the linear fit, which represents the second border case of particles with constant surface area (infinite plates). The comparison with the experimental data shows that up to 60% conversion both fits describe the course of reaction almost similar. For a conversion of up to 90% (60 min < t < 90 min), the shrinking core model assuming spherical particles fails, while the linear fit assuming flat particle gets unsatisfying above 100 min. As generally the easier but still accurate model shall be chosen, it is assumed that for the given powder up to 90% TiC conversion the kinetics can be described by the flat plate model. Fig. 2 shows a SEM image of the untreated titanium carbide powder. The particles seem to be rather platelets with high aspect ratios that spheres, which support that the conversion of these particles can be describe up to high degrees of conversion by a flat plate model. The strong decrease of the reaction rate during the last 10% of conversion may origin to some amount from the 8% of particles with a bigger size (between 9.3 and 24 μm) or from inclusions of carbides covered with some layers of non-porous carbon which are only slowly chlorinated at the end of the reaction. For the further discussion of the kinetics in the next chapters, this does not have to be taken into account, because only experiments with less than 90% conversion were used to determine the kinetic parameters. Then the total etching rate is still represented by Eq. (1), and this mean integral rate of an experiment can be regarded as the actual reaction rate.

The N_2-sorption analysis shows the strong increase of the specific surface area with increasing conversion (Fig. 3). This can be explained well by the assumption, that the surface area is practically only supplied by the porous carbon and not by the unconverted carbide. The total specific surface area can then be calculated by the mass content of carbon and the total specific surface area of pure carbon. The mass content of the carbon is a function of the degree of conversion of the carbide, while the specific surface area of the carbon A_C remains as fitting parameter:

$$A_{TiC+C}(X_{TiC}) = A_C \frac{m_C}{m_C + m_{TiC}} = A_C \frac{X_{TiC}(M_C/M_{TiC})}{X_{TiC}(M_C/M_{TiC}) + (1 - X_{TiC})} \tag{7}$$

Fig. 3 clearly indicates that Eq. (7) describes the experimental data very well if the specific surface area at complete conversion is set within the fit to 1470 m^2/g. Hence a high degree of TiC conversion is essential to produce carbide-derived carbons with high specific surface areas of more than 1000 m^2/g, and 36% of the specific surface area are created during the last 10% of conversion (the difference in the molar mass of titanium carbide and carbon is responsible for this behavior).

Beside the total specific surface area also the pore size distribution is interesting. The mean pore size is calculated according to Eqs. (8) and (9) from the pore size distribution obtained from N_2-sorption measurement and NL-DFT calculations. The pore size distribution shows mainly micropores and probably some mesopores below 10 nm.

$$d_{v,\text{mean}} = \frac{\sum_{0\ \text{nm}}^{10\ \text{nm}} \overline{d_i} \cdot v_i}{\sum_{0\ \text{nm}}^{10\ \text{nm}} v_i} \tag{8}$$

$$d_{a,\text{mean}} = \frac{\sum_{0\ \text{nm}}^{10\ \text{nm}} \overline{d_i} \cdot a_i}{\sum_{0\ \text{nm}}^{10\ \text{nm}} a_i} \tag{9}$$

with $\overline{d_i}$: mean pore diameter of interval i in m; v_i: specific volume of interval i in m^3/kg; a_i: specific area of interval i in m^2/kg.

The mean pore sizes obtained at different degrees of TiC conversion (Table 2) shows that the mean pore diameter is almost constant, at least for a conversion of more than about 20%. In the initial phase of the reaction, the meso- or macroporosity of the titanium carbide powder has an influence on the measured mean pore size. The untreated carbide shows a specific volume of 0.011 ml/g with a volume averaged mean pore size of 4.89 nm, which influences the mean pore size at lower conversions. To obtain the mean pore size diameter of the porous carbon only, the specific surface area and specific volume of each interval of the pore size distributions were reduced by the specific surface area or volume of the untreated carbide powder. The resulting corrected volume averaged mean pore sizes are also given in Table 2, which indicate that the mean pore size of the carbon has a constant value of around 0.64 nm. Hence it can be concluded that the pore structure of the

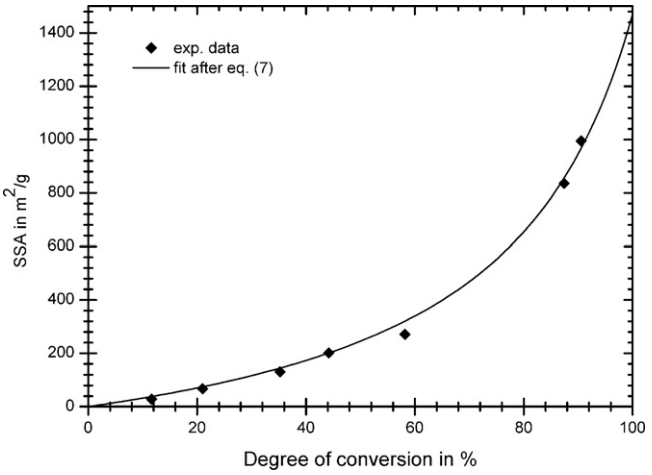

Fig. 3. Specific surface areas derived from N_2-sorption measurement and NL-DFT calculations over the degree of conversion ($c_{Cl_2,0}$ = 0.45 mol/m^3, T = 800 °C) and fit after Eq. (7).

Table 2
Volume and area averaged mean pore size derived from N_2-sorption measurement and NL-DFT calculations over the degree of TiC conversion ($c_{Cl_2,0} = 0.45\,mol/m^3$, $T = 800\,^\circ C$).

X [%]	0	21.0	35.2	44.2	58.2	87.5	90.6
Volume averaged mean pore size [nm]	4.89	1.12	0.79	0.87	0.79	0.65	0.74
Corrected volume averaged mean pore size of carbon [nm]		0.56	0.66	0.67	0.65	0.60	0.69
Area averaged mean pore size [nm]	4.0	0.75	0.62	0.64	0.62	0.58	0.60

carbon which is obtained in the beginning of the reaction is not influence further by the ongoing reaction. This would happen for example by the reaction of the carbon with chloride to gaseous CCl_4.

The influence of the TiC conversion on the true density was evaluated by helium pycnometry (Fig. 4). As expected, a linear decrease of the apparent density starting from the density of titanium carbide can be observed. The true density is given by

$$\rho_{true}(X) = \rho_{TiC} \cdot (1 - X) + \rho_{carbon} \cdot X \quad (10)$$

with ρ_{true}: true density of the partially reacted substrate; ρ_{TiC}: $4930\,kg/m^3$; ρ_{carbon}: fit results to $2907\,kg/m^3$.

The true density of the synthesized carbon as obtained from the fit shown in Fig. 4 is $2907\,kg/m^3$. Hence for example for quality control in an industrial process the conversion can be estimated by helium pycnometry which is a relative fast analysis.

3.2. Influence of reaction temperature

A variation of the reaction temperature at constant reaction time and initial chlorine concentration (30 min, $c_{Cl_2,0} = 0.45\,mol/m^3$) only leads to small increase of the rate with temperature (Fig. 5). The degree of conversion was thereby less than 35%, i.e. the total etching rate can be calculated by Eq. (1). The activation energy is only 6.5 kJ/mol. Despite the low activation energy typical for diffusion limitations, external mass transfer limitations can be neglected because the rate is very slow and in Chapter 3.1 it was also shown that internal mass transfer limitations are also negligible. From the order of magnitude of the activation energy a limitation of the diffusion of reactants within a non-porous solid could be responsible and the rate depending step, but an explanation for the rather low activation energy cannot be given up to now.

An increase in temperature beyond 800 °C even leads to a slight drop of the reaction rate. This could be for example attributed to a change in the reaction mechanism and intermediate steps of the etching reaction, but also the porosity and the degree of crystallization of the carbon may change with temperature, which could also have an impact on the etching rate.

The N_2-sorption measurements show (Table 3) that the specific surface area doubles for an increase of the temperature from 400 to 800 °C, which cannot only be attributed to the small increase of conversion from 25% to 35%. At higher temperatures the specific surface area drops dramatically. From the corrected volume averaged mean pore size of the carbon (see Chapter 3.1) it can be seen that the mean pore size of the carbon is bigger at temperatures below 600 °C and above 800 °C. Thus, microporous carbon with a sharp pore size distribution is only obtained in a range from 600 to 800 °C. For lower temperatures, the increase of the mean pore size is probably the result of carbon which is etched via gaseous CCl_4 and may lead to a pore widening. For further confirmation it would be necessary to analyze the product gas for CCl_4, which was not possible with the given setup.

The Raman spectras in Fig. 6 show that at higher temperatures the ratio of intensities (I_D/I_G), the ratio of the areas (A_D/A_G), and the

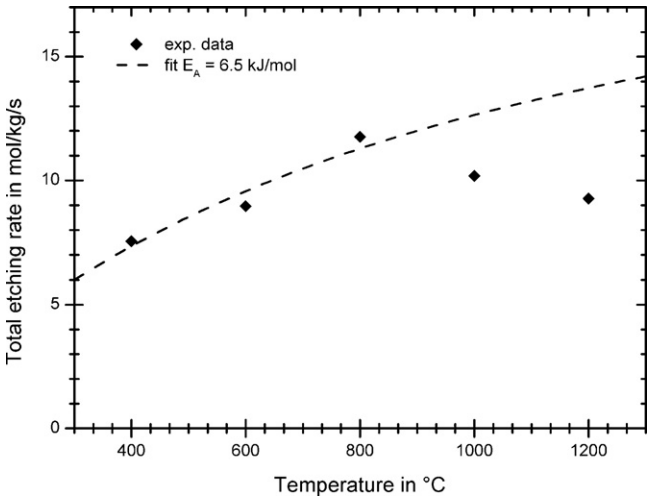

Fig. 5. Etching rate of TiC at different temperatures (30 min, $c_{Cl_2,0} = 0.45\,mol/m^3$, $25\% < X < 35\%$).

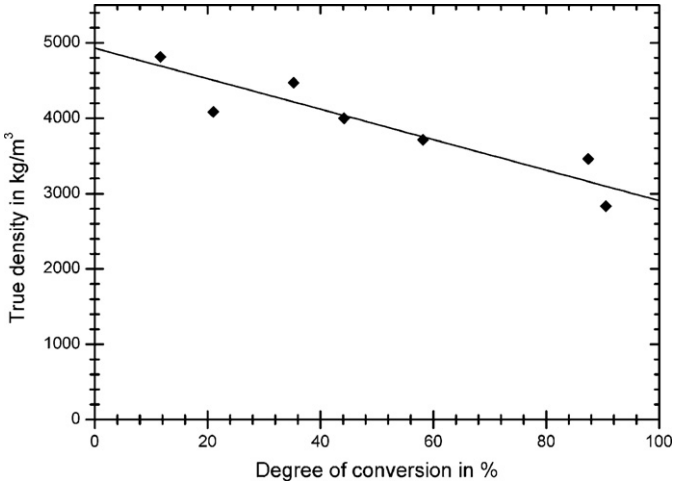

Fig. 4. Development of the apparent density determined by helium pycnometriy ($c_{Cl_2,0} = 0.45\,mol/m^3$, $T = 800\,^\circ C$).

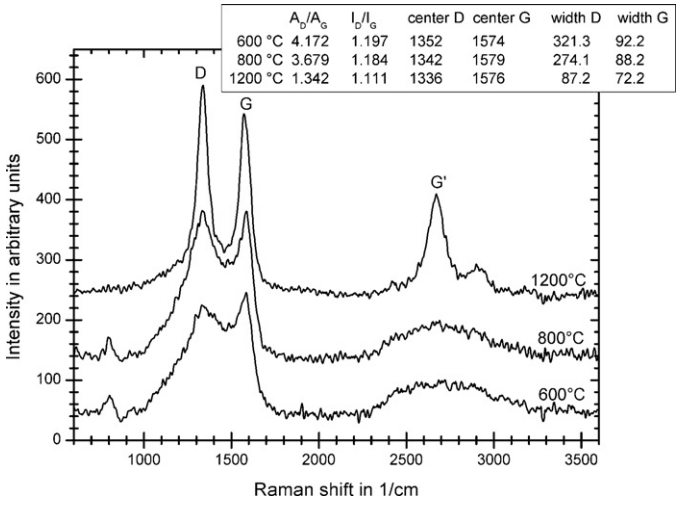

Fig. 6. Raman spectra of TiC-DC obtained at different temperatures.

Table 3
Volume and area averaged mean pore size derived from N_2-sorption measurement and NL-DFT calculations over the degree of conversion (30 min, $c_{Cl_2,0} = 0.45\,mol/m^3$, 25% < X < 35%).

T [°C]	400	600	800	1000	1200
Volume averaged mean pore size [nm]	2.20	0.90	0.84	2.73	4.83
Corrected volume averaged mean pore size of carbon [nm]	1.84	0.48	0.53	2.53	4.83
Area averaged mean pore size [nm]	1.09	0.63	0.63	1.77	4.44
Specific surface area [m^2/g]	62.0	100.2	130.2	56.5	7.3

peak widths decrease. This indicates that the carbon becomes more ordered at higher temperatures. This reordering could be responsible for the creation of mesopores [33,34]. A similar increase of the mean pore size for higher reaction temperatures was also reported in literature [35–37].

A final conclusion about the origin of the uncommon dependency of the total rate on the reaction temperature cannot be given in this work. Detailed studies about the product composition at reaction temperature could reveal information about the reaction mechanism and probable changes. Also it needs to be clarified if strong mass transfer limitations, which are not a function of the conversion and growing nanoporous film, like dissolution and diffusion of chlorine inside of the solid at the reaction front, are present.

3.3. Influence of the chlorine concentration

The chlorine concentration was varied at a constant superficial velocity, reaction time and temperature in a range of 0.22–6.6 mol/m^3 ($u = 0.015$ m/s, $t = 10$ min or 30 min, $T = 800$ °C). Fig. 7 shows the plot of the total etching rate versus the chlorine concentration. For the first six data points with an initial chlorine concentration below 1.35 mol/m^3 the conversion increases from 12% to 85%. The experiment with a concentration of 6.6 mol/m^3 was performed with a reaction time of 10 min (instead of 30 min), which led to a conversion of 82%. Thus, the assumption of a constant etching rate is still valid as shown in Fig. 1.

Before the reaction rate approach is derived, it has to be checked if the change of the chlorine concentration within the tubular reactor can be neglected. Two moles of chlorine are consumed for each mole of titaniumtetrachloride, and hence the chlorine concentration at the reactor outlet is given by:

$$c_{Cl_2,outlet} = \frac{c_{Cl_2,0} \cdot f_{Cl_2}}{1 - 0.5 \cdot (1 - f_{Cl_2})} \quad \text{with}$$

$$f_{Cl_2} = \frac{\dot{n}_{0,Cl_2} \cdot t - n_{Ti}}{\dot{n}_{0,Cl_2} \cdot t} = \frac{\dot{n}_{0,Cl_2} \cdot t - (\Delta m / M_{Ti})}{\dot{n}_{0,Cl_2} \cdot t} \tag{11}$$

The concentration of chlorine at the reactor outlet and the resulting depletion of the concentration along the crucible filled with carbide powder is given in Table 4. Due to slightly different initial masses of carbide powder, the chlorine conversion varied in a range 30–40%. Due to the change in volume the depletion of the chlorine concentration is small and below 25%. Therefore, the observed non-linear behavior of the reaction rate (Fig. 7) cannot be attributed to the consumption of the reactant.

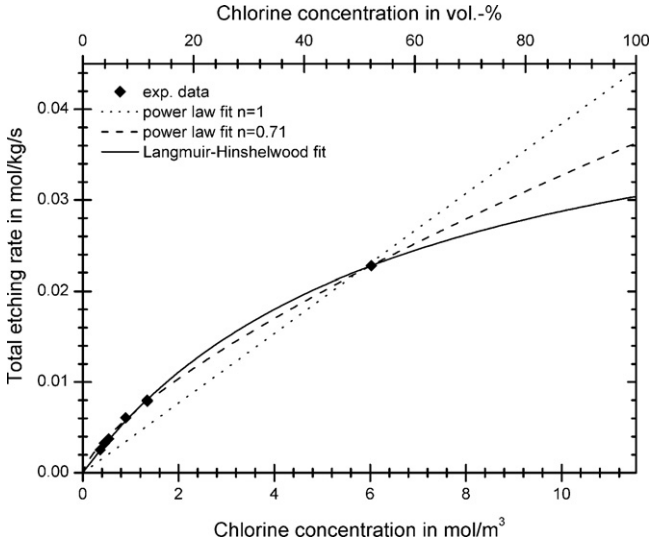

Fig. 7. Etching rate and fits for different chlorine concentrations ($T = 800$ °C, $t = 30$ min, data at 6.6 mol/m^3 for $t = 10$ min).

As gaseous chlorine reacts with solid titanium carbide, an adsorption step of chlorine, consecutive reaction and desorption step of $TiCl_4$ could be thought of. Hence the number of adsorption sides and equilibrium loadings can have an impact on the reaction rate, like it is described commonly by the Langmuir–Hinshelwood approach. Fig. 7 shows the good fit which can be achieved by this assumption and resulting reaction rate approach:

$$r_{total,LH} = \frac{0.151\,(m^3/mol) \cdot 4.48 \cdot 10^{-2}\,mol/(kg\,s) \cdot c_{Cl_2}}{1 + 0.151\,(m^3/mol) \cdot c_{Cl_2}} \tag{12}$$

Alternatively, a simple power law approach can also be used to describe the kinetics for chlorine concentration quite well below 11.2 mol/m^3 (pure chlorine at 1 bar and 800 °C). The reac-

Table 4
Calculated concentrations of chlorine at the reactor outlet.

$c_{Cl_2,0}$ [mol/m^3]	0.22	0.36	0.45	0.54	0.90	1.35	6.62
X_{Cl_2} [%]	29.4	39.2	35.0	39.3	38.9	33.7	30.6
$c_{Cl_2,outlet}$ [mol/m^3]	0.19	0.28	0.35	0.41	0.68	1.07	5.43
Depletion of c_{Cl_2} [%]	17.2	24.4	21.2	24.5	24.1	20.2	18.0

Table 5
Volume and area averaged mean pore size derived from N_2-sorption measurement and NL-DFT calculations for different chlorine concentrations resulting in different degrees of TiC conversion ($t = 30$ min, $T = 800$ °C).

$c_{Cl_2,0}$ [mol/m^3]	0.22	0.36	0.45	0.54	0.90	1.35
X [%]	12	27	35	40	65	85
Volume averaged mean pore size [nm]	1.68	0.96	0.79	0.89	0.68	0.66
Corrected volume averaged mean pore size of carbon [nm]	0.76	0.58	0.66	0.67	0.56	0.61
Area averaged mean pore size [nm]	0.96	0.67	0.62	0.65	0.58	0.58

tion order is then 0.71, and the value of the rate constant 6.3×10^{-3} $mol^{0.29}$ $m^{2.31}/kg/s$.

The influence of the chlorine concentration on the reaction rate shows that the synthesis can only be accelerated to a small extent by employing pure chlorine gas for the CDC-process. Thus the chlorination with diluted chlorine gas can be economical advantageous. Secondly, it can be observed that up to pure chlorine atmosphere (11.2 mol/m^3 at 800 °C) a power law approach is sufficient for the kinetic description. For this approach a description of the diffusion and reaction steps in series is simpler than for the Langmuir–Hinshelwood approach. Experimental and mathematical considerations about the influence of the growing nanoporous carbon layer on the reaction rate will be published elsewhere.

The sorption analysis shows that the specific surface area increases with increasing chlorine concentration, which can be attributed to the rise in conversion. The evolution of the mean pore size indicates that the pore size is not influenced by the chlorine concentration (Table 5).

4. Conclusions

In this work a detailed kinetic study about the chlorination of titanium carbide powder for the synthesis of carbide-derived carbons is presented. No limitation by external or internal mass transfer was observed for the employed 3.5 μm powder.

The specific surface area increases non-linear with the degree of conversion and is created mainly in the last 10%. Thus, an almost complete conversion is needed to obtain carbon with a high specific surface area. The true density decreases linearly with increasing conversion. Equations describing both values as a function of conversion are given.

As described in the literature the reaction temperature has a strong influence on the resulting pore size distribution and specific surface area. Surprisingly, only a minor influence on the reaction rate was observed. The rate follows a Langmuir–Hinshelwood approach, which can be simplified to a power law approach with an order of 0.71 regarding chlorine. The chlorine concentration has no influence on the mean pore size and specific surface area.

Acknowledgements

This report is based on a project which was funded by E.ON AG as part of the E.ON International Research Initiative. Responsibility for the content of this publication lies with the author. The authors gratefully acknowledge the funding of the German Research Council (DFG), which, within the framework of its 'Excellence Initiative', supports the Cluster of Excellence 'Engineering of Advanced Materials' (www.eam.uni-erlangen.de) at the University of Erlangen-Nuremberg.

References

[1] O. Vohler, G. Nutsch, G. Collin, F.V. Sturm, E. Wege, W. Frohs, K.-D. Henning, H.V. Kienle, M. Voll, P. Kleinschmit, O. Vostrowsky, A. Hirsch, Carbon, in: Ullmann's Encyclopedia of Industrial Chemistry, Wiley-VCH, Weinheim, 2009.
[2] P. Serp, J.L. Figueiredo, Carbon Materials for Catalysis, 1st ed., John Wiley & Sons, Hoboken, 2009.
[3] M. Rossberg, W. Lendle, G. Pfleiderer, A. Tögel, E.-L. Dreher, E. Langer, H. Rassaerts, P. Kleinschmidt, H. Strack, R. Cook, U. Beck, K.-A. Lipper, T.R. Torkelson, E. Löser, K.K. Beutel, T. Mann, Chlorinated hydrocarbons, in: Ullmann's Encyclopedia of Industrial Chemistry, Wiley-VCH, Weinheim, 2009.
[4] J. Wisniak, M. Klein, Reduction of nitrobenzene to aniline, Ind. Eng. Chem. Prod. Res. Dev. 23 (1984) 44.
[5] A. Nieto-Marquez, S. Gil, A. Romero, J.L. Valverde, S. Gomez-Quero, M.A. Keane, Gas phase hydrogenation of nitrobenzene over acid treated structured and amorphous carbon supported Ni catalysts, Appl. Catal. A 363 (2009) 188.
[6] A. Nikitin, Y. Gogotsi, Nanostructured carbide-derived carbon, in: Encyclopedia of Nanoscience and Nanotechnology, American Scientific Publishers, 2004.
[7] Y. Gogotsi, I.D. Jeon, M.J. McNallan, Carbon coatings on silicon carbide by reaction with chlorine-containing gases, J. Mater. Chem. 7 (1997) (1841).
[8] Y. Gogotsi, A. Nikitin, H. Ye, W. Zhou, J.E. Fischer, B. Yi, H.C. Foley, M.W. Barsoum, Nanoporous carbide-derived carbon with tunable pore size, Nat. Mater. 2 (2003) 591.
[9] A. Jänes, T. Thomberg, E. Lust, Synthesis and characterisation of nanoporous carbide-derived carbon by chlorination of vanadium carbide, Carbon 45 (2007) 2717.
[10] A. Jänes, T. Thomberg, H. Kurig, E. Lust, Nanoscale fine-tuning of porosity of carbide-derived carbon prepared from molybdenum carbide, Carbon 47 (2009) 23.
[11] P. Gupta, M.J. McNallan, Water vapor absorption on nanostructured carbide derived carbon (CDC), ECS Trans. 6 (2007) 71.
[12] M. Seredych, C. Portet, Y. Gogotsi, T.J. Bandosz, Nitrogen modified carbide-derived carbons as adsorbents of hydrogen sulfide, J. Colloid Interface Sci. 330 (2009) 60.
[13] S.H. Yeon, S. Osswald, Y. Gogotsi, J.P. Singer, J.M. Simmons, J.E. Fischer, M.A. Lillo-Ródenas, A. Linares-Solano, Enhanced methane storage of chemically and physically activated carbide-derived carbon, J. Power Sources 191 (2009) 560.
[14] Y. Gogotsi, R.K. Dash, G. Yushin, T. Yildirim, G. Laudisio, J.E. Fischer, Tailoring of nanoscale porosity in carbide-derived carbons for hydrogen storage, J. Am. Chem. Soc. 127 (2005) 16006.
[15] G. Yushin, R. Dash, J. Jagiello, J.E. Fischer, Y. Gogotsi, Carbide-derived carbons: effect of pore size on hydrogen uptake and heat of adsorption, Adv. Funct. Mater. 16 (2006) 2288.
[16] R. Dash, J. Chmiola, G. Yushin, Y. Gogotsi, G. Laudisio, J. Singer, J. Fischer, S. Kucheyev, Titanium carbide derived nanoporous carbon for energy-related applications, Carbon 44 (2006) 2489.
[17] C. Portet, J. Chmiola, Y. Gogotsi, S. Park, K. Lian, Electrochemical characterizations of carbon nanomaterials by the cavity microelectrode technique, Electrochim. Acta 53 (2008) 7675.
[18] A. Jänes, L. Permann, M. Arulepp, E. Lust, Electrochemical characteristics of nanoporous carbide-derived carbon materials in non-aqueous electrolyte solutions, Electrochem. Commun. 6 (2004) 313.
[19] A. Jänes, E. Lust, Electrochemical characteristics of nanoporous carbide-derived carbon materials in various nonaqueous electrolyte solutions, J. Electrochem. Soc. 153 (2006).
[20] R. Lin, P.L. Taberna, J. Chmiola, D. Guay, Y. Gogotsi, P. Simon, Microelectrode study of pore size, ion size, and solvent effects on the charge/discharge behavior of microporous carbons for electrical double-layer capacitors, J. Electrochem. Soc. 156 (2008).
[21] C. Portet, M.A. Lillo-Rodenas, A. Linares-Solano, Y. Gogotsi, Capacitance of KOH activated carbide-derived carbons, Phys. Chem. Chem. Phys. 11 (2009) 4943.
[22] J. Chmiola, G. Yushin, Y. Gogotsi, C. Portet, P. Simon, P.L. Taberna, Anomalous increase in carbon at pore sizes less than 1 nanometer, Science 313 (2006) (1760).
[23] J. Torop, M. Arulepp, J. Leis, A. Punning, U. Johanson, A. Aabloo, Low voltage linear actuators based on carbide-derived carbon powder, Proc. SPIE-Int. Soc. Opt. Eng. 7287 (2009).
[24] J. Chmiola, G. Yushin, R. Dash, Y. Gogotsi, Effect of pore size and surface area of carbide derived carbons on specific capacitance, J. Power Sources 158 (2006) 765.
[25] M. McNallan, D. Ersoy, R. Zhu, A. Lee, C. White, S. Welz, Y. Gogotsi, A. Erdemir, A. Kovalchenko, Nano-structured carbide-derived carbon films and their tribology, Tsinghua Sci. Technol. 10 (2005) 699.
[26] E.N. Hoffman, G. Yushin, B.G. Wendler, M.W. Barsoum, Y. Gogotsi, Carbide-derived carbon membrane, Mater. Chem. Phys. 112 (2008) 587.
[27] Y. Gogotsi, R.K. Dash, G. Yushin, B.E. Carroll, S.R. Altork, S. Sassi-Gaha, R.F. Rest, Bactericidal activity of chlorine-loaded carbide-derived carbon against *Escherichia coli* and *Bacillus anthracis*, J. Biomed. Mater. Res., Part A 84 (2008) 607.
[28] M. Kormann, H. Gerhard, N. Popovska, Comparative study of carbide-derived carbons obtained from biomorphic TiC and SiC structures, Carbon 7 (2009) 242.
[29] M. Kormann, H. Ghanem, H. Gerhard, N. Popovska, Processing of carbide-derived carbon (CDC) using biomorphic porous titanium carbide ceramics, J. Eur. Ceram. Soc. 28 (2008) 1297.
[30] A. Lee, R. Zhu, M. McNallan, Kinetics of conversion of silicon carbide to carbide derived carbon, J. Phys.: Condens. Matter 18 (2006).
[31] D.A. Ersoy, M.J. McNallan, Y. Gogotsi, Carbon coatings produced by high temperature chlorination of silicon carbide ceramics, Mater. Res. Innovat. 5 (2001) 55.
[32] Z.G. Cambaz, G.N. Yushin, Y. Gogotsi, K.L. Vyshnyakova, L.N. Pereselentseva, Formation of carbide-derived carbon on b-silicon carbide whiskers, J. Am. Ceram. Soc. 89 (2006) 509.
[33] S. Urbonaite, L. Hälldahl, G. Svensson, Raman spectroscopy studies of carbide derived carbons, Carbon 46 (2008) (1942).
[34] M. Kormann, H. Gerhard, C. Zollfrank, H. Scheel, N. Popovska, Effect of transition metal catalysts on the microstructure of carbide-derived carbon, Carbon 47 (2009) 2344.
[35] G. Laudisio, R.K. Dash, J.P. Singer, G. Yushin, Y. Gogotsi, J.E. Fischer, Carbide-derived carbons: a comparative study of porosity based on small-angle scattering and adsorption isotherms, Langmuir 22 (2006) 8945.
[36] S. Urbonaite, J.M. Juárez-Galán, J. Leis, F. Rodríguez-Reinoso, G. Svensson, Porosity development along the synthesis of carbons from metal carbides, Microporous Mesoporous Mater. 113 (2008) 14.
[37] P. Zetterström, S. Urbonaite, F. Lindberg, R.G. Delaplane, J. Leis, G. Svensson, Reverse Monte Carlo studies of nanoporous carbon from TiC, J. Phys.: Condens. Matter. 17 (2005) 3509.